Thin Solid Films 807 (2024) 140544

Contents lists available at ScienceDirect

Thin Solid Films

journal homepage: www.elsevier.com/locate/tsf

Comprehensive quantifying of the Fe-Ti-B film magnetic microstructure

E.V. Harin [a,*], E.N. Sheftel [a], V.A. Tedzhetov [a], D.M. Gridin [b], V.V. Popov [b], T.P. Kaminskaya [b], A.B. Granovsky [b,c]

[a] Baikov Institute of Metallurgy and Materials Science RAS, 119334, Moscow, Russia
[b] Lomonosov Moscow State University, 119992, Moscow, Russia
[c] Institute for Theoretical and Applied Electromagnetics RAS, 125412, Moscow, Russia

ARTICLE INFO

Keywords:
Magnetron deposition
Nanocrystalline film ferromagnet
Random anisotropy model
Correlation magnetometry
Magnetic force microscopy
Magnetic microstructure
Magnetic properties

ABSTRACT

Investigation and quantifying of the parameters of the phase and structure state, static magnetic properties, magnetic microstructure formed over the entire volume of the film and in the near-surface layer, the surface roughness of $Fe_{72.4}Ti_{5.4}B_{19.2}O_{3.0}$ film were carried out using the combination of the methods such as x-ray diffraction, magnetic force microscopy, atomic force microscopy, vibrating-sample magnetometry, and the correlation magnetometry. The $Fe_{72.4}Ti_{5.4}B_{19.2}O_{3.0}$ films on glass substrates were produced by magnetron deposition followed by the vacuum annealing at 200 °C for 1 h. The interrelation between the investigated parameters was highlighted.

1. Introduction

The magnetic properties of nanocrystalline soft magnetic films are determined by many material characteristics, including the phase composition and structure, the magnetic microstructure formed over the entire volume of the film (volume magnetic microstructure), the macroscopic magnetic anisotropy [1-3] and in the near-surface layer [4], the roughness [5] and phase composition of the film surface [6]. Therefore, the investigations aimed at the study and quantification of the specified characteristics formed in the conditions of obtaining films, finding their interrelation with each other and with the magnetic properties of films are of scientific and practical importance for targeted designing of films, which provide the properties required for modern magnetoelectronics [1,2].

There are various methods of the study of above mentioned characteristics of the nanocrystalline ferromagnetic films: (i) microscopic techniques, such as the Lorentz microscopy, Kerr microscopy, magnetic force microscopy (MFM), and magnetic small-angle neutron scattering, which are suitable for the observation of near-surface magnetic microstructure [4], (ii) correlation magnetometry, based on the analysis of approach to saturation magnetization [3], which allows one to describe the volume magnetic microstructure and (iii) X-ray diffraction (XRD) analysis, which allows one to determine the grain size of material, microstrain within a grain, and macrostresses in films. The data obtained by a combination of these methods on the same material provides a possibility to identify various sources determining the value of the film coercive field H_c and the saturation magnetization M_s, as the most important applied properties of the soft magnetic films.

The macroscopic magnetic anisotropy of nanocrystalline ferromagnets is considered in terms of random anisotropy model (RAM) [7]. According to RAM, when the grain size $2R_c$ is less than the exchange interaction length R_L, the randomly oriented local magnetic anisotropy (at the scale $2R_c$) is suppressed by exchange interaction at the stochastic domain scale $2R_L$; the stochastic domain size is determined by the competition between the rms fluctuation of local magnetic anisotropy field $D^{1/2}H_a$ and exchange interaction. It should be noted that, in the case of absence of other magnetic anisotropy sources in addition to $D^{1/2}H_a$ in the magnetic structure (such as macrostresses [8], exchange stiffness inhomogeneities [9], etc.) the equality of the coercive field and the rms fluctuation of effective magnetic anisotropy of stochastic domain $D^{1/2}\langle H_a\rangle$ at the $2R_L$ scale can be satisfied [3]: $H_c \approx D^{1/2}\langle H_a\rangle$.

According to the scientifically substantiated approach, developed by us for choosing the compositions of nanocrystalline films being able to meet the properties required for modern magnetoelectronics [10], the films of the Fe-Ti-B alloys are promising [11,12]. This fact determines the use of the Fe-Ti-B films for achieving the goal of the study.

In this regard, the goal of this work was to study and quantify the phase and structural state of the Fe-Ti-B films, obtained under certain

* Corresponding author.
E-mail address: ekharin@imet.ac.ru (E.V. Harin).

https://doi.org/10.1016/j.tsf.2024.140544
Received 5 June 2024; Received in revised form 23 September 2024; Accepted 25 September 2024
Available online 26 September 2024

conditions of magnetron deposition with subsequent annealing, its volume and near-surface magnetic microstructure, as well the roughness of the film surface. The goal of the work was also to establish the relationship of these characteristics with each other and with the static magnetic properties of the films.

2. Material and methods

The Fe-Ti-B films were prepared by magnetron sputtering of composite target (5-inch diameter), which comprise a Fe disk (110 cm^2 in area) uniformly coated with TiB_2 ceramic segments 21 cm^2 in total area (the ceramics was prepared by self-propagating high-temperature synthesis). The films were deposited on heat-proof silica glass substrates 50 × 50 mm in size and 1 mm in thickness for 10 min in an Ar atmosphere at a pressure of 0.3 Pa, a cathode voltage of 500 V, and a current of 1.5 A. The substrate temperature was measured using a resistance temperature detector (Pt100) mounted on the substrate holder. During the deposition process, the substrate-holder was heated from room temperature to 205 °C under the influence of plasma. No separate heater was used for the substrates. The deposition conditions are given in detail in [12]. The films were annealed at 200 °C for 1 h at a residual gas pressure of 2 × 10^{-4} Pa. It was shown in the previous our work [11] that the combination of the highest M_s and the lowest H_c values is achieved after annealing at 200 °C for 1 h in Fe-Ti-B films of compositions similar to those studied in this work.

The chemical composition (Fe 72.4, Ti 5.4, B 19.2, O 3.0 at.%) and the thickness ($d = 0.52 \pm 0.03$ μm) of the films were determined using a Hitachi S3400N scanning electron microscope equipped with a Noran 7 Thermo Scientific system, applying an acceleration voltage of 20 kV and a vacuum of 7 × 10^{-4} Pa. Atomic fractions of elements were calculated using Hall's continuum method with an error of determination no more than 1.6 at.%. Such thick films were chosen for three reasons: (i) the presence of out-of-plane magnetization increases the contrast in magnetic force microscopy (Section 3.3); (ii) the film thickness is much larger than the grain size, which allows observing the law of approach to saturation in its pure form (Section 3.4), without low-dimensional and fractal asymptotes intermediate between $H^{-1/2}$ and H^{-2} and a noticeable influence of surface anisotropy; (iii) the "transcritical" shape of the hysteresis loop (Section 3.2) allows analytical calculation of the width of the stripe domains based on indirect measurements (Section 3.5), which width was compared with measurements from the MFM and from the approach to saturation magnetization.

The phase analysis and the fine structure of the studied films were performed by XRD, transmission electron microscopy (TEM) and electron diffraction (ED). XRD patterns were taken in Bragg-Brentano geometry in a 2θ angular range of 30 to 90° at a step of 0.04° using a Rigaku Ultima IV diffractometer equipped with a graphite monochromator and CuK_α radiation; a scintillation detector was used to record radiation. The obtained patterns were approximated by Lorentz function. The grain thickness (grain size) was calculated using the Scherrer equation. It is known that the XRD method allows one to estimate the coherent-scattering domain size by the magnitude of the broadening of diffraction reflections [13]. For nanocrystalline alloys, the grain thickness (grain size) estimation by the XRD method is widely used and gives good agreement with the data of "direct" methods [14-16] including the papers of the authors of the present article, devoted to the film alloys with similar nanostructure [17].

The structure of films was also studied by TEM and ED using Tecnai G^2 30ST and FEI Osiris electron microscopes. Samples for the electron-microscopic studies were prepared in the form of cross sections and in-plane samples. The thinning was performed with specific pasts, sprays, and argon ions with an energy of 3–5 keV and an incident angle of 3–5° using a Gatan PIPS 691 system. The processing and analysis of TEM images was fulfilled using Digital Micrograph and TIA software. The grain-size distribution was estimated using ImageScope software.

MFM was carried out in two-pass mode using a NT-MDT Smena atomic force microscope (AFM) in semi-contact mode using a Co-coated cantilever with resonant frequencies 47–90 kHz and force constants 1–5 N/m; the second pass was fulfilled at a height of 100 nm above the surface; the sampling rate was 256 pixels/line. AFM and MFM images were processed in the NOVA program using the Image Analysis P9 image processing module.

Magnetic hysteresis loops were measured at room temperature in magnetic fields of up to 1280 kA/m (16 kOe) using a LakeShore 7407 vibrating-sample magnetometer. Magnetic field was applied in the film plane and along the normal to the surface (out-of-plane). The volume magnetic microstructure was studied by correlation magnetometry method [3].

3. Results and discussion

3.1. Phase composition and structure

Fig. 1 shows experimental XRD patterns taken for the films under study. There is a single very wide reflection centered near 44°, locating near the position of the (110) reflection of αFe ($2\theta_{(110)} = 44.72°$) on the XRD patterns taken for the as-deposited film. The lattice parameter of the phase calculated using the angular position of the wide reflection is 2.873 ± 0.003 Å and is significantly exceed that of αFe (2.866 Å). It means that a mixed (nanocrystalline + amorphous) structure containing the Fe-based phase is formed in the as-deposited films. Considering that Ti dissolves in αFe (3 at.% at 25 °C and 10 at.% at 1289 °C) to form the solid solution αFe(Ti) in equilibrium systems [18], as well that the concentration range of solid solution existence expands in metastable systems obtained by high-energy synthesis [19], it is natural to believe that the solid solution αFe(Ti) is formed in the as-deposited films. The annealing leads to a decrease in the integral width of the wide reflection located near 44° (from 6.65 to 5.96°), a shift in the angular position of this reflection towards that for αFe (from 44.57 to 44.61°), as well as the appearance of the second very weak wide reflection centered near 2θ~55°. It means that the annealing at 200 °C for 1 h leads to the following transformations:

(i) the partial crystallization of the amorphous phase;
(ii) the appearance of new grains of the Fe based phase;
(iii) the partial depletion of the Fe-based phase with Ti as evidenced by the decrease in the parameter value of the αFe-based phase from 2.873 ± 0.003 Å to 2.870 ± 0.003 Å; the latter is consistent with increasing grain thickness (grain size) from 7 ± 1 to 11 ± 2 nm in the annealed films;
(iv) the appearance of the additional Fe_3B phase (the reflex near 2θ~55° corresponds to the position of the reflex from the Fe_3B phase) instead of the TiB_2 phase which is expected according to the equilibrium phase diagram Fe-Ti-B [18]. It is known that the phase composition of films obtained by high energy synthesis (including magnetron deposition) is metastable and may not correspond to that predicted by the equilibrium phase diagram due to the predominance of kinetic factors over thermodynamic ones.

According to TEM and ED data, columnar agglomerates oriented along the film growth direction with nanosized grains of the αFe-based phase located in columns are observed in the annealed films (Fig. 2b). The αFe-based phase is evidenced by the strongly diffused rings corresponding to this phase on the ED (Fig. 1c). The columns as is known [20, 21] are agglomerates of nanocrystalline grains of the same orientation.

3.2. Magnetic hysteresis loops

The shape of magnetic hysteresis loops of the studied films (the low relative remanence about 0.14 and almost linear portion of hysteresis loop in fields above H_c, Fig. 2a) indicates the existence of high uniaxial

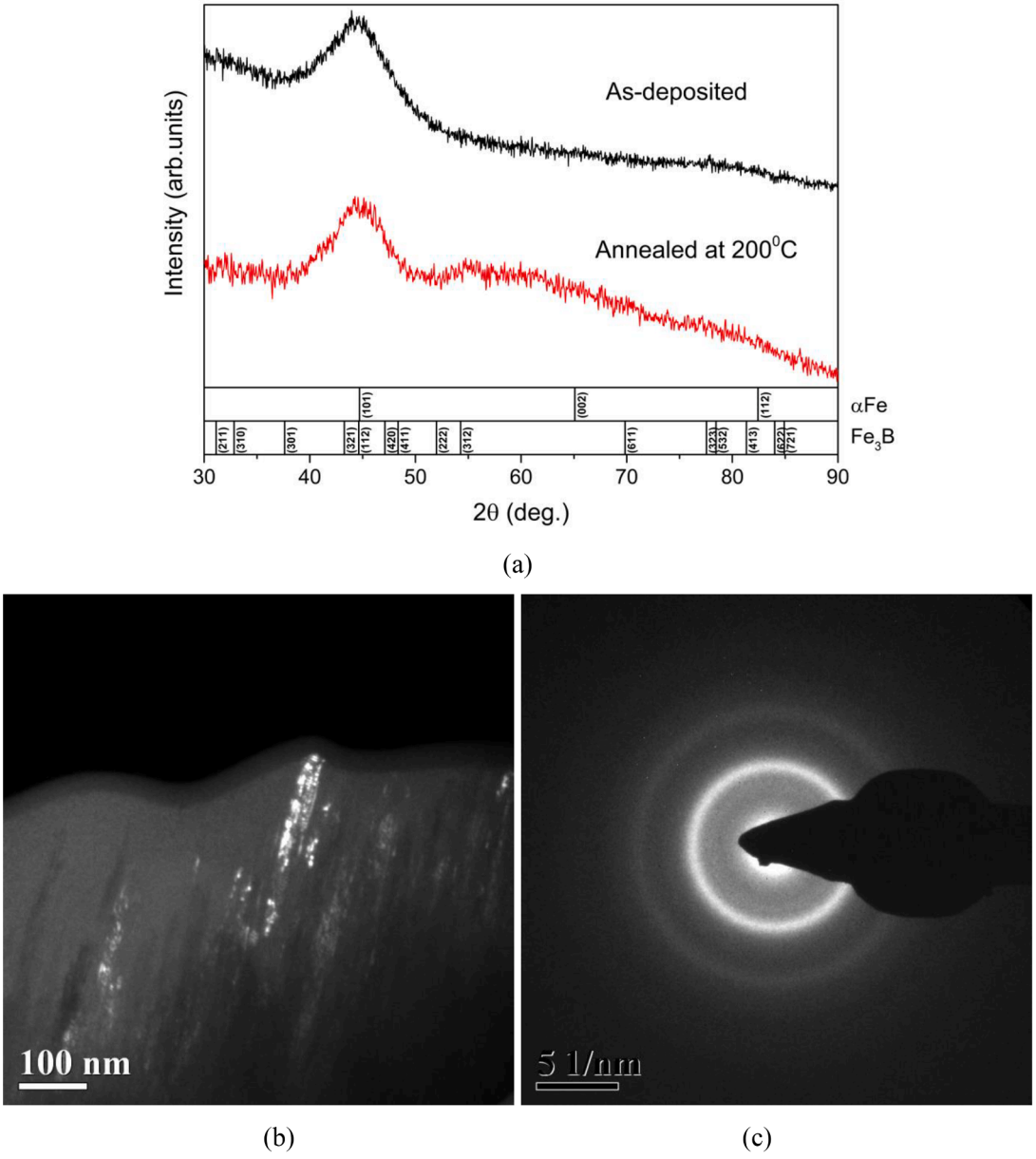

Fig. 1. (a) XRD patterns of the studied films in the as-deposited state and annealed at 200 °C; (b) dark-field image and (c) associated ED pattern obtained for the films after annealing.

magnetic anisotropy, which is likely to be related to the columnar structure (Fig. 1b). The columnar structure is usually formed in such films under magnetron sputtering [22]. The annealing leads to the substantial changes in the hysteresis loop shape, that are observed in the region of approach to saturation (above 80 kA/m) and near the origin of coordinates (the inset in Fig. 2a). The changes in the region of approach to saturation are described in Section 3.4.

The annealing leads to the increase (within the measurement accuracy) of H_c and M_s from 2 ± 0.16 to 2.4 ± 0.16 kA/m (from 25 ± 2 to 30 ± 2 Oe) and from 1.8 ± 0.1 to 2.00 ± 0.14 T (from 1400 ± 80 to 1600 ± 110 G), respectively. The hysteresis loop of the annealed film near the origin of coordinates is characterized by an anomaly in the form of a bend corresponding to a field about 800 A/m (10 Oe). This fact indicates the presence of two magnetic phases differing in the coercive field (the inset in Fig. 2a) which is consistent with the data obtained by XRD (Section 3.1) on the formation of two ferromagnetic phases, αFe(Ti) and Fe_3B.

To determine the coercive field of each of the magnetic anisotropies (H_{c1} and H_{c2}), the loops (open circles in the inset in Fig. 2a) were described by the empirical function which can be considered as the modification of classical Langevin formula [23] for magnetization process:

$$M(H) = M_{s1}V_1\left(\coth(P_1(H \pm H_{c1})) - (P_1(H \pm H_{c1}))^{-1}\right) + M_{s2}V_2\left(\coth(P_2(H \pm H_{c2})) - (P_2(H \pm H_{c2}))^{-1}\right) + \chi H,$$

where *coth* is hyperbolic cotangent, P_1, P_2, $M_{s1}V_1$, $M_{s2}V_2$ and χ are the adjustable parameters. Note that the hysteresis loop is the magnetic moment of the sample divided by its volume. If there are two phases in a film with different saturation magnetizations, they are summed in proportion to their volume fractions V_1 and V_2. Since XRD gave us information about two ferromagnetic phases (αFe(Ti) and Fe_3B) with close saturation magnetization values (differing by less than 20 %: 2.0 ± 0.14 and 1.6 T [24], respectively), it is impossible to distinguish their saturation magnetizations, i.e. M_{s1} and M_{s2} cannot be identified with specific quantities. Considering the closeness of the saturation magnetization

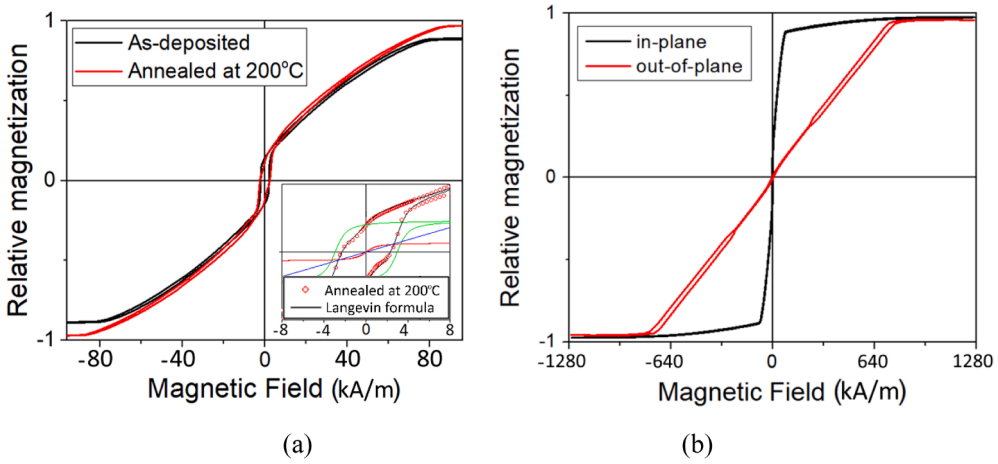

Fig. 2. (a) Hysteresis loops of the studied films in the as-deposited state and annealed at 200 °C, the inset shows the hysteresis loop of the annealed film (open circles) and the terms (green, red, and blue solid lines) of the Langevin formula (black solid lines); (b) in-plane and out-of-plane hysteresis loops of the studied film in the as-deposited state.

values ($M_{s1} \approx M_{s2}$), the volume fractions (V_1 and V_2) of the two magnetizations are equal to about 0.14 and 0.04 and their coercive fields (H_{c1} and H_{c2}) are equal to about 3 and 0.08 kA/m (37 and 1 Oe), respectively.

In the case where the film does not have perpendicular anisotropy (i.e., magnetization lies in the film plane in the absence of an external field), when an external field is applied normally to the film plane, a linear magnetization curve with a saturation field of $4\pi M_s$ should be

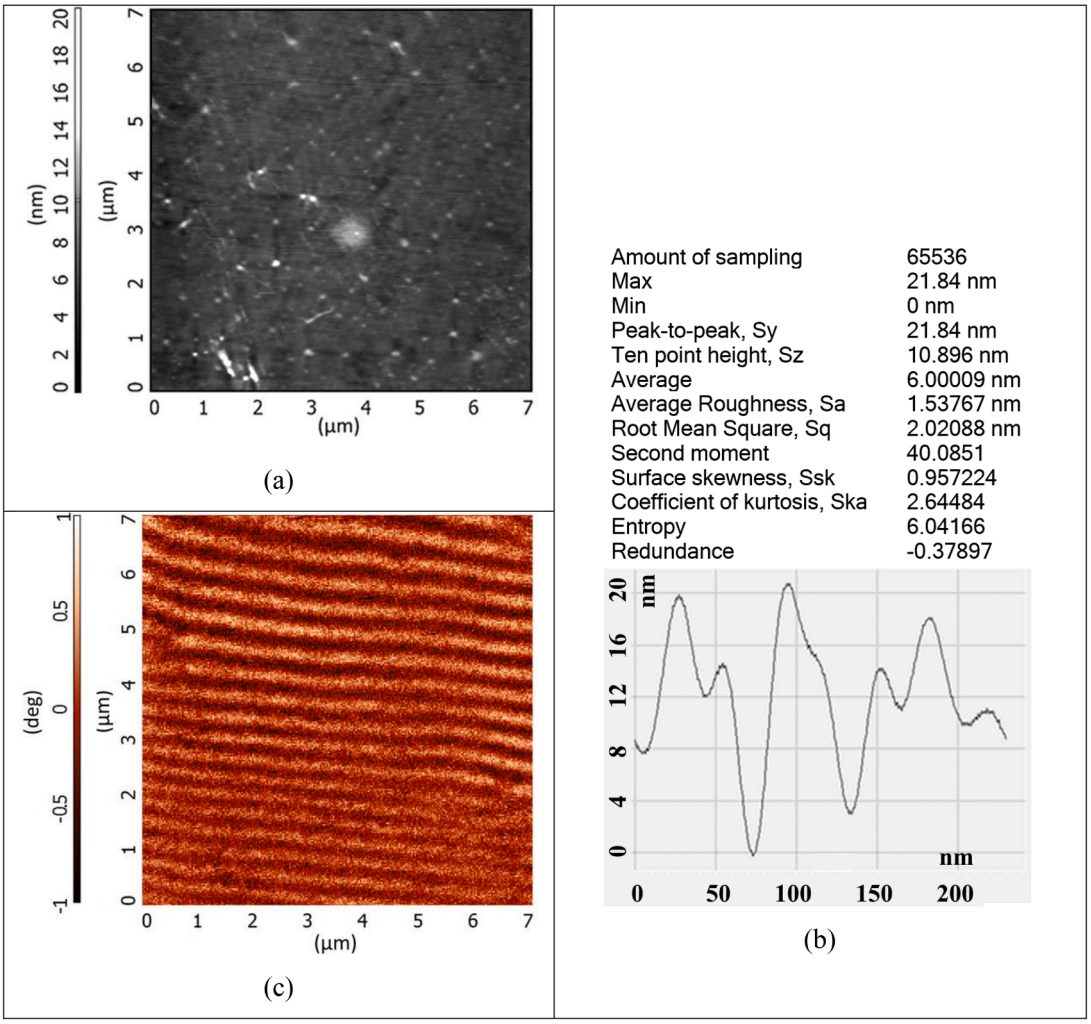

Fig. 3. (a) AFM image of the film surface; (b) the statistical treatment of the data of surface heterogeneity and the average profile along *x*-axis on AFM image; (c) and MFM image of the studied film annealed at 200 °C.

observed. For the studied films in the as-deposited state $4\pi M_s = 1400 \pm 80$ kA/m (17.6 ± 1.0 kOe). However, out-of-plane magnetization measurements (Fig. 2b) showed a saturation field about 760 kA/m (9.5 kOe), which is significantly less than $4\pi M_s$. The possible reason could be related to the measurement artefacts related to centering procedure for out-of-plane measurement in the films.

3.3. Near-surface magnetic microstructure

The film annealed at 200 °C was studied by AFM (Fig. 3a) and MFM (Fig. 3c). The statistical treatment (Fig. 3b) of the data of surface heterogeneity showed the rms roughness of about 2 nm, the peak-to-peak (about 22 nm), and the average roughness (p = 6 nm). The average size of in-plane surface heterogeneity is equal to 60 ± 10 nm (Fig. 3b shows the average profile along x-axis), being greater than the roughness height by an order of magnitude. This indicates the existence of a columnar structure reaching the film surface (see Section 3.1). As was noted in Section 3.2, columnar structure affects the shape of hysteresis loops (Fig. 2). The film surface heterogeneity formed by the columns (Fig. 1b) creates an additional demagnetizing with the anisotropy field [25] (in cgs units) $H_u = 4\pi^2 M_s p^2/(\lambda d)$, where λ is the dominate wavelength of roughness (doubled size of the in-plane surface heterogeneity) and d is the film thickness. The H_u value, calculated using the M_s, p, λ, d values measured in the work, is 2.6 ± 1.8 kA/m (32 ± 22 Oe), which is close to the value of the measured H_c = 2.4 ± 0.16 kA/m (Fig. 2a). It means that H_c value is mainly determined by the contribution to the magnetic anisotropy of the columns consisting of nanosized grains of the αFe (Ti) phase. Apparently, the contribution from the Fe_3B phase formed during annealing at 200 °C is too insignificant due to its small amount.

The contrast in the MFM image (Fig. 3c) indicates magnetic field gradient above the film surface. This magnetic field gradient reflects the projection of relative magnetization distribution along the normal to the film surface in the absence of external field. Therefore, the clear contrast observed in Fig. 3c means the presence of out-of-plane magnetization component, which can manifest itself in the hysteresis loops as almost linear portion of hysteresis loop in fields above H_c (Fig. 2a). The statistical treatment of the image given in Fig. 3c allowed us to determine the stripe domain width that is equal to 420 ± 20 nm.

3.4. Volume magnetic microstructure

The correlation magnetometry method makes it possible to determine the parameters of the magnetic microstructure ($D^{1/2}\langle H_a\rangle$, $D^{1/2}H_a$, and $2R_L$) of amorphous and nanocrystalline films, averaged over the entire volume, using the magnetization curves in the region of approach to saturation (the inset in Fig. 4). According to the correlation magnetometry method [3], the experimentally measured magnetization curve in high magnetic fields (the inset in Fig. 4) was fitted by

$$M(H) = M_s\left[1 - (1/2)\left(D^{1/2}H_a\right)^2 \Big/ \left(H^2 + H^{1/2}H_R^{3/2}\right)\right] \quad (1)$$

Using Eq. (1) and setting the field H equal to infinity, we quantify the M_s value that allowed us to find the values of $D^{1/2}H_a$ and exchange field H_R before annealing ($D^{1/2}H_a$ = 200 ± 16 kA/m and H_R = 448 ± 64 kA/m) and after it ($D^{1/2}H_a$ = 96 ± 10 kA/m and H_R = 592 ± 74 kA/m, respectively). According to data of [3], the field H_R (in cgs units) $H_R = A/(M_s R_c^2)$, where A is the effective exchange stiffness) is the threshold value of field $D^{1/2}H_a$: at $D^{1/2}H_a < H_R$ the exchange interaction between grains leads to the formation of stochastic domains. The D value, which is the easy-axis magnetic anisotropy dispersion, depends on the local magnetic anisotropy symmetry, and for the uniaxial anisotropy is 1/15.

The correctness of determination of $D^{1/2}H_a$ and H_R values was checked by the graphical correlation magnetometry method. For this purpose, the dependence of magnetization dispersion $d_m = 1 - M/M_s$ (the M_s value was determined to a high accuracy by Eq. (1)) on the external field H, was plotted on log-log scale (Fig. 4). The red curve (Fig. 4),

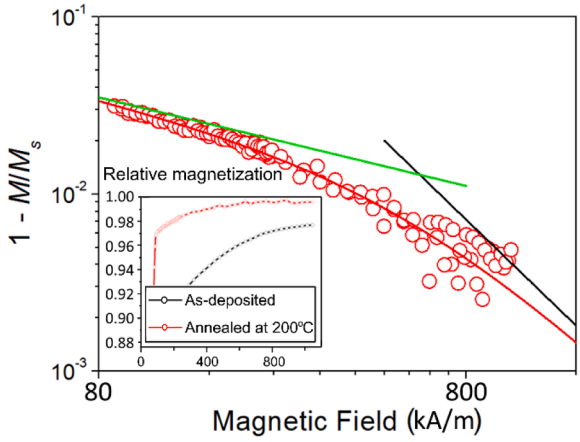

Fig. 4. Magnetization dispersion $d_m = 1 - M/M_s$ of the film annealed at 200 °C. Solid red line corresponds to fitting of experimental data (circles) by Eq. (1) and black and green lines are asymptotes $(1/2)(D^{1/2}H_a/H)^2$ and $(1/2)(D^{1/2}H_a)^2/(H^{1/2}H_R^{3/2})$, respectively. The inset shows magnetization curves measured before and after annealing.

corresponding to Eq. (1), has two asymptotes, namely, a black line is $d_m = (1/2)(D^{1/2}H_a/H)^2$ known as the Akulov's law, which was used to determine the field $D^{1/2}H_a$, and a green line is $d_m = (1/2)(D^{1/2}H_a)^2/(H^{1/2}H_R^{3/2})$, which indicates the decrease in the stochastic domain size with increasing field H (up to the disappearance of exchange interaction between grains at $H > H_R$). The H_R field corresponds to the field of intersection of these asymptotes.

Knowing the $D^{1/2}H_a$ and H_R values, the field $D^{1/2}\langle H_a\rangle = (D^{1/2}H_a)^4/H_R^3$ = 400 ± 240 A/m (5 ± 3 Oe) was estimated for the annealed film. The observed bend on the hysteresis loop of the annealed film (Fig. 2a) reflects the coercive field of the softer magnetic phase, and this coercive field is close to the value of $D^{1/2}\langle H_a\rangle$.

The relative stochastic domain size is $R_L/R_c = (H_R/D^{1/2}H_a)^2$ = 39 ± 14 for the annealed film. For this film $D^{1/2}H_a < H_R$ and therefore $R_L/R_c > 1$; this indicates the existence of exchange interaction between ferromagnetic grains. Allowing the grain thickness (grain size) of annealed film equal to $2R_c$ = 11 ± 2 nm (see Section 3.1), the stochastic domain size is $2R_L$ = 430 ± 30 nm. This value is quite close to the stripe domain width determined by MFM (see Section 3.3).

3.5. Out-of-plane magnetic anisotropy

The columnar structure directed normal to the film surface (see Section 3.1) creates magnetic anisotropy in which the easy axis of magnetization is directed along the length of the columns. This perpendicular magnetic anisotropy is in competition with the demagnetizing field, which tends to hold the magnetization in the film plane. Therefore, the out-of-plane magnetization strongly depends on the perpendicular magnetic anisotropy and may occur for quite thick films depending on their microstructure. In the case of soft magnetic films (similar to permalloy), the out-of-plane magnetization component occurs at a film thickness of 100–1000 nm [26-32].

Along with the stripe domain structure (Fig. 3), the close to linear portion of hysteresis loops in fields above H_c observed after annealing (Fig. 2a) and characterized by the saturation field H_s = 88 ± 8 kA/m (1100 ± 100 Oe) indicates the fact that the film is in "transcritical" state, i.e., its thickness d is higher than L_{cr}. The critical thickness $L_{cr} = 2\pi(A/K_p)^{1/2}$, where K_p is the out-of-plane magnetic anisotropy constant (in this case, the easy axis is perpendicular to the film plane) [26]. In a film with the thickness being less than L_{cr}, the demagnetizing field holds whole magnetization in the film plane. Knowing the H_s value from the hysteresis loop, K_p is determined from the expression (in cgs units) $H_s = (K_p/M_s)[1-(2\pi(A/K_p)^{1/2}/d)(1+K_p/(2\pi M_s^2))^{-1/2}]$ [27,28], where A =

10^{-11} J/m (10^{-6} erg/cm). At this H_s value, K_p is equal to $(1 \pm 0.1)\bullet 10^5$ J/m^3 (10^6 erg/cm^3). Then L_{cr} is equal to 63 ± 3 nm at this K_p value. The calculated value $L_{cr} < d$ confirms that the film is in "transcritical" state.

Knowing the calculated K_p value, the out-of-plane magnetic anisotropy field H_p is determined from the expression $H_p = 2K_p/M_s = 100 \pm 9.6$ kA/m (1250 ± 120 Oe). This value is close to local anisotropy field determined by correlation magnetometry method (see Section 3.4).

Knowing the K_p value, the stripe domain width can be determined by the expression (in cgs units) $D_m = d^{1/2}[\pi A(K_p+2\pi M_s^2)/(2K_pM_s^2)]^{1/4}$ [27, 29]. It is equal to $D_m = 130 \pm 3$ nm and is lower than that determined by MFM and correlation magnetometry methods (Sections 3.3 and 3.4). This is related to three simultaneous facts: (i) the out-of-plane magnetic anisotropy observed experimentally is not ideally perpendicular [26], (ii) the near-surface magnetic microstructure differs from the volume one, and (iii) the possible existence of in-plane magnetic anisotropy, since according to MFM data the orientation of stripe domains changes over the film surface at the scale of several μm.

4. Conclusions

The $Fe_{72.4}Ti_{5.4}B_{19.2}O_{3.0}$ films on glass substrates were obtained by magnetron deposition. The mixed (nanocrystalline + amorphous) structure containing αFe(Ti) phase is formed in the as-deposited film. The vacuum annealing at 200 °C for 1 h leads to partial crystallization of the amorphous phase accompanied by the appearance of new grains of the αFe(Ti) phase and additional Fe_3B phase. The αFe(Ti)-phase grain thickness (7–11 nm) is determined by XRD. The saturation magnetization M_s and the coercive field H_c of the as-deposited films are 1.8 ± 0.1 T (1400 ± 80 G) and 2 ± 0.16 kA/m (25 ± 2 Oe), respectively. Annealing leads to the increase of M_s to 2.00 ± 0.14 T (1600 ± 110 G) and H_c to 2.4 ± 0.16 kA/m (30 ± 2 Oe). The existence of extensive linear portion in the hysteresis loops and stripe domain structure observed by MFM testifies the formation of columnar structure in the films. Wherein the average size of the in-plane surface heterogeneity (60 ± 10 nm) corresponds to the column thickness reaching the film surface. The stochastic domain size (430 ± 30 mn) determined by correlation magnetometry is close to the width of stripe domain structure observed by MFM. The correctness of quantifying the volume magnetic microstructure by indirect correlation magnetometry method is demonstrated. The role of magnetic microstructure parameters in the formation mechanism of coercive field, which is the main characteristic of the magnetic softness of alloys, was estimated.

CRediT authorship contribution statement

E.V. Harin: Writing – review & editing, Writing – original draft, Validation, Methodology, Investigation, Formal analysis. **E.N. Sheftel:** Writing – review & editing, Writing – original draft, Project administration, Methodology, Investigation, Formal analysis, Conceptualization. **V.A. Tedzhetov:** Writing – original draft, Software, Resources, Investigation. **D.M. Gridin:** Writing – review & editing, Software, Resources, Formal analysis. **V.V. Popov:** Writing – review & editing, Supervision, Software, Methodology. **T.P. Kaminskaya:** Writing – review & editing, Visualization, Validation, Software, Resources, Methodology. **A.B. Granovsky:** Writing – review & editing, Supervision, Resources, Project administration, Methodology, Formal analysis, Data curation.

Declaration of competing interest

The authors declare that they have no known competing financial interests or personal relationships that could have appeared to influence the work reported in this paper.

Data availability

Data will be made available on request.

Acknowledgements

The authors express their gratitude to Dr.Sc. Zhigalina O.M. (National Research Centre "Kurchatov Institute") for assistance in conducting research using TEM and ED methods.

The study was financially supported by the Russian Science Foundation under project no. 23-23-00434 (https://rscf.ru/en/project/23-23-00434/).

References

[1] J. Zhou, J. You, K. Qiu, Advances in Fe-based amorphous/nanocrystalline alloys, J. Appl. Phys. 132 (2022) 040702.
[2] G. Scheunert, O. Heinonen, R. Hardeman, A. Lapicki, M. Gubbins, R.M. Bowman, A review of high magnetic moment thin films for microscale and nanotechnology applications, Appl. Phys. Rev. 3 (2016) 011301.
[3] S.V. Komogortsev, R.S. Iskhakov, Law of approach to magnetic saturation in nanocrystalline and amorphous ferromagnets with improved transition behavior between power-law regimes, J. Magn. Magn. Mater. 440 (2017) 213–216.
[4] N.G. Chechenin, A.R. Chezan, C.B. Craus, T. Vystavel, D.O. Boerma, J.Th.M. de Hosson, L. Niesen, Microstructure of nanocrystalline FeZr(N) films and their soft magnetic properties, J. Magn. Magn. Mater. 242–245 (2002) 180–182.
[5] J. Gong, S. Riemer, M. Kautzky, I. Tabakovic, Composition gradient, structure, stress, roughness and magnetic properties of 5–500 nm thin NiFe films obtained by electrodeposition, J. Magn. Magn. Mater. 398 (2016) 64–69.
[6] Y. Yu, J. Shi, Y. Nakamura, Roles of interface roughness and internal stress in magnetic anisotropy of CoPt/AlN multilayer films, Acta Mater. 60 (2012) 6770–6778.
[7] G. Herzer, Modern soft magnets: amorphous and nanocrystalline materials, Acta Mater. 61 (2013) 718–734.
[8] E.V. Harin, E.N. Sheftel, Micromagnetic structure of soft magnetic nanocrystalline Fe-based films, Phys. Metals Metall. 116 (2015) 753–759.
[9] B.P. Khrustalev, A.D. Balaev, V.G. Pozdnyakov, L.I. Vershinina, The spin-wave resonance spectrum and the structure of cermet Fe-SiO films, Solid State Commun. 55 (1985) 657–662.
[10] E.N. Sheftel, V.A. Tedzhetov, E.V. Harin, G.Sh. Usmanova, Films with nanocomposite structure αFe(N) +ZrN for soft magnetic applications, Thin Solid Films 748 (2022) 139146.
[11] E.N. Sheftel, V.A. Tedzhetov, E.V. Harin, F.V. Kiryukhantsev-Korneev, G. Sh. Usmanova, High-induction nanocrystalline soft magnetic $Fe_XTi_YB_Z$ films prepared by magnetron sputtering, Phys. Status Solidi C 13 (2016) 965–971.
[12] E.N. Sheftel, V.A. Tedzhetov, Ph.V. Kiryukhantsev-Korneev, E.V. Harin, G. Sh. Usmanova, O.M. Zhigalina, Investigation of the processes of the formation of a nonequilibrium phase-structural state in FeTiB films obtained by magnetron sputtering, Russian J. Non-Ferrous Metals 61 (2020) 753–761.
[13] B.E. Warren, X-ray Diffraction, Addison-Wesley Publishing Company, Reading, MA, USA, 1969, p. 230.
[14] I. Feijoo, M. Cabeza, P. Merino, G. Pena, M.C. Pérez, S. Cruz, P. Rey, Estimation of crystallite size and lattice strain in nano-sized TiC particle-reinforced 6005A aluminium alloy from X-ray diffraction line broadening, Powder Technol. 343 (2019) 19–28.
[15] H. Jensen, J.H. Pedersen, J.E. Jorgensen, J.S. Pedersen, K.D. Joensen, S.B. Iversen, E.G. Sogaard, Determination of size distributions in nanosized powders by TEM, XRD, and SAXS, J. Exp. Nanosci. 1 (2006) 355–373.
[16] D. Louer, J.P. Auffredic, J.I. Langford, D. Ciosmak, J.C. Niepce, A precise determination of the shape, size and distribution of size of crystallites in zinc oxide by X-ray line-broadening analysis, J. Appl. Cryst. 16 (1983) 183–191.
[17] E.N. Sheftel, V.A. Tedzhetov, E.V. Harin, P.V. Kiryukhantsev-Korneev, G. S. Usmanova, O.M. Zhigalina, FeZrN films: magnetic and mechanical properties relative to the phase-structural state, Materials 15 (2022) 137.
[18] J.L. Murray, The Fe-Ti (iron-titanium) system, Bull. Alloy Phase Diagr. 2 (1981) 320–334.
[19] R. Arnell, R. Bates, The deposition of highly supersaturated metastable aluminium-magnesium alloys by unbalanced magnetron sputtering from composite targets, Vacuum 43 (1992) 105–109.
[20] P.B. Barna, M. Adamik, Formation and characterization of the structure of surface coatings, in: Y. Paleau, P.B. Barna (Eds.), Protective Coatings and Thin Films, Kluwer Academic, Dordrecht, The Netherlands, 1997, pp. 279–297.
[21] G. Radnóczi, P. Barna, Formation and characterization of the structure of thin films and coatings, in: Y. Pauleau (Ed.), Materials Surface Processing by Directed Energy Techniques, Elsevier, Amsterdam, The Netherlands, 2006, pp. 443–474.
[22] E.N. Sheftel, V.A. Tedzhetov, E.V. Harin, P.V. Kiryukhantsev-Korneev, O. M. Zhigalina, G.S. Usmanova, Magnetron deposited FeTiB films: from structural metastability to the specific magnetic state, Coatings 14 (2024) 475.
[23] S.V. Komogortsev, E.A. Denisova, R.S. Iskhakov, A.D. Balaev, L.A. Chekanova, Yu. E. Kalinin, A.V. Sitnikov, Multilayer nanogranular films $(Co_{40}Fe_{40}B_{20})_{50}(SiO_2)_{50}$/α-Si:H and $(Co_{40}Fe_{40}B_{20})_{50}(SiO_2)_{50}/SiO_2$: magnetic properties, J. Appl. Phys. 113 (2013) 17C105.
[24] R. Coehoorn, D.B. De Mooij, C. De Waard, Meltspun permanent magnet materials containing Fe_3B as the main phase, J. Magn. Magn. Mater. 80 (1989) 101–104.
[25] E. Schlömann, Demagnetizing fields in thin magnetic films due to surface roughness, J. Appl. Phys. 41 (1970) 1617–1623.

[26] S.V. Komogortsev, I.G. Vazhenina, S.A. Kleshnina, R.S. Iskhakov, V.N. Lepalovskij, A.A. Pasynkova, A.V. Svalov, Advanced characterization of FeNi-based films for the development of magnetic field sensors with tailored functional parameters, Sensors 22 (2022) 3324.
[27] P.N. Solovev, A.V. Izotov, B.A. Belyaev, N.M. Boev, Micromagnetic simulation of domain structure in thin permalloy films with in-plane and perpendicular anisotropy, Phys. B Condens. Matter 604 (2021) 412699.
[28] Y. Sugita, H. Fujiwara, T. Sato, Critical thickness and perpendicular anisotropy of evaporated permalloy films with stripe domains, Appl. Phys. Lett. 10 (1967) 229–231.
[29] Y. Murayama, Micromagnetics on stripe domain films. I. Critical cases, J. Phys. Soc. Jpn. 21 (1966) 2253–2266.
[30] A.V. Svalov, A.N. Gorkovenko, A. Larrañaga, M.N. Volochaev, G.V. Kurlyandskaya, Structural and magnetic properties of FeNi films and FeNi-based trilayers with out-of-plane magnetization component, Sensors 22 (2022) 8357.
[31] A.R. Chezan, C.B. Craus, N.G. Chechenin, T. Vystavel, L. Niesen, J.Th.M. De Hosson, D.O. Boerma, Influence of stresses and magnetostriction on the soft magnetic behavior of metallic films, J. Magn. Magn. Mater. 299 (2006) 219–224.
[32] N. Cotón, J.P. Andrés, M. Jaafar, A. Begué, R. Ranchal, Tuning the out-of-plane magnetic textures of electrodeposited $Ni_{90}Fe_{10}$ thin films, J. Appl. Phys. 135 (2024) 093905.